This article was downloaded by:
On: *25 January 2011*
Access details: *Access Details: Free Access*
Publisher *Taylor & Francis*
Informa Ltd Registered in England and Wales Registered Number: 1072954 Registered office: Mortimer House, 37-41 Mortimer Street, London W1T 3JH, UK

Liquid Crystals
Publication details, including instructions for authors and subscription information:
http://www.informaworld.com/smpp/title~content=t713926090

Twin-like domains in chiral smectic C liquid crystals

Monique Brunet[a]; Lubor Lejček[b]; Laurence Navailles[c]; Patrick Keller[d]; Tinh Huu Nguyen[c]; Eric Polossat[a]; Emmanuel Rouy[a]
[a] Laboratoire des Colloides, Verres et Nanomateriaux, UMR 5587, Université Montpellier II, 34095 Montpellier, France [b] Institute of Physics, Academy of Sciences of the Czech Republic, 182 21 Prague 8, Czech Republic [c] CRPP, 33600 Pessac, France [d] Laboratoire Physico-Chimie Curie, UMR CNRS 168, Institut Curie-Section de Recherche, 75231 Paris Cedex 05, France

To cite this Article Brunet, Monique , Lejček, Lubor , Navailles, Laurence , Keller, Patrick , Nguyen, Tinh Huu , Polossat, Eric and Rouy, Emmanuel(2006) 'Twin-like domains in chiral smectic C liquid crystals', Liquid Crystals, 33: 9, 961 — 978
To link to this Article: DOI: 10.1080/02678290600816965
URL: http://dx.doi.org/10.1080/02678290600816965

PLEASE SCROLL DOWN FOR ARTICLE

Full terms and conditions of use: http://www.informaworld.com/terms-and-conditions-of-access.pdf

This article may be used for research, teaching and private study purposes. Any substantial or systematic reproduction, re-distribution, re-selling, loan or sub-licensing, systematic supply or distribution in any form to anyone is expressly forbidden.

The publisher does not give any warranty express or implied or make any representation that the contents will be complete or accurate or up to date. The accuracy of any instructions, formulae and drug doses should be independently verified with primary sources. The publisher shall not be liable for any loss, actions, claims, proceedings, demand or costs or damages whatsoever or howsoever caused arising directly or indirectly in connection with or arising out of the use of this material.

Liquid Crystals, Vol. 33, No. 9, September 2006, 961–978

Taylor & Francis
Taylor & Francis Group

Twin-like domains in chiral smectic C liquid crystals

MONIQUE BRUNET†, LUBOR LEJČEK*‡, LAURENCE NAVAILLES§, PATRICK KELLER¶, TINH HUU NGUYEN§, ERIC POLOSSAT† and EMMANUEL ROUY†

†Laboratoire des Colloides, Verres et Nanomateriaux, UMR 5587, Université Montpellier II, 34095 Montpellier, France
‡Institute of Physics, Academy of Sciences of the Czech Republic, Na Slovance 2, 182 21 Prague 8, Czech Republic
§CRPP, Av. A. Schweitzer, 33600 Pessac, France
¶Laboratoire Physico-Chimie Curie, UMR CNRS 168, Institut Curie-Section de Recherche, 11 rue P. et M. Curie, 75231 Paris Cedex 05, France

(*Received 15 August 2005; in final form 5 April 2006; accepted 19 April 2006*)

In the chiral smectic C phase of liquid crystals with the phase transition N*–SmC*, texture development depending on the sample thickness is reported. In very thin samples, domains of rectangular-like shape are observed. As two possible tilts of smectic layers are possible for one anchoring direction, smectic layers inside a domain, called twin-like domains, are tilted with respect to layers in outer regions, similarly to crystalline planes in solid crystalline twins. An elastic model of such a twin domain is proposed and its energy determined.

Downloaded At: 15:54 25 January 2011

1. Introduction

The textures observed in chiral smectic C (SmC*) liquid crystals with the phase sequence chiral nematic (N*)–chiral smectic C (SmC*) differ from those in the SmC* with the more common sequence chiral nematic (N*)–chiral smectic A (SmA*)–chiral smectic C (SmC*). The phase sequence N*–SmC* is generally of the first order with an almost temperature independent molecular tilt angle θ [1], which can attain rather high values, $\sim 45^\circ$ [2, 3]. Alignment properties and the layer reorientation induced by an external electric field have previously been investigated [1–6]. The study of molecular alignment in smectic layers showed the existence of two possible orientations of the layer normal, inclined from the rubbing direction by angles $\pm\theta$. Therefore the layer structure can form 'horizontal chevrons' [5, 7].[†] Planes of horizontal chevrons (chevron interfaces [8]) with opposite layer inclinations form domains usually of rectangular or parallelogram shape. These domains are reminiscent of twins in solid crystals. Horizontal chevron interfaces are similar to coherent twin boundaries in solids because the layers change the inclination without a layer discontinuity. Domains are closed by planes of layer discontinuities which will be termed incoherent walls. Such domains, similar to twins in solids [9] which were also observed in [10], will be further called twin-like domains. A similar situation to that described can also appear in a non-chiral SmC phase at the phase transition N–SmC.

This paper consists of two parts. In the first part (§2, 3) the observation of SmC* or SmC textures created during the phase transition from N* or N to SmC* or SmC will be reported. The observations show differences in layer structures depending on the cell thickness. While in very thin samples relatively simple twin-like textures are seen, in thicker samples very complex structures like focal conics in various orientations were revealed. The layer orientation of thicker samples was investigated by X ray diffractometry. These observations are followed by discussions and attempts at interpretation.

In the second part of this paper (§4) an approximate elastic model of a twin-like domain is constructed, which allows us to describe such a twin-like domain in thin or thicker SmC* or SmC samples, and to determine its elastic energy. The energy of so-called coherent walls can be determined using the methods of [11]. The incoherent wall can be described by a dislocation model [13].

*Corresponding author. Email: brunetmonique@numericable.fr, lejcekl@fzu.cz; this paper is dedicated to Professor Sven T. Lagerwall on the occasion of his 70th birthday.

[†]If we suppose the glass plates of the cell to be horizontal, a 'horizontal chevron' is oriented in such a way that the smectic layer intersections define a plane which is vertical; that is, perpendicular to the glass plates. Even for X-ray experiments, where the glass plates are vertical, we will continue to call this chevron, a 'horizontal chevron'. By comparison a 'vertical chevron' is oriented in such a way that the chevron plane is parallel to the glass plates.

Liquid Crystals
ISSN 0267-8292 print/ISSN 1366-5855 online © 2006 Taylor & Francis
http://www.tandf.co.uk/journals
DOI: 10.1080/02678290600816965

2. Experimental

The present study of textures in the SmC* phase of materials exhibiting the N*–SmC* phase sequence was performed on samples of different thicknesses (D) and with different aligning layers, filled into cells in the isotropic state. The compounds used to fill the cells were either commercial mixtures — ZLI 3079 from Merck, Chisso 2004, which are SmC* at room temperature — or a pure compound synthesized by T.H. Nguyen with the phase sequence I–80°C–N*–64°C–SmC*–43°C–Cr, which we will call $C_9^* H_{19}$.

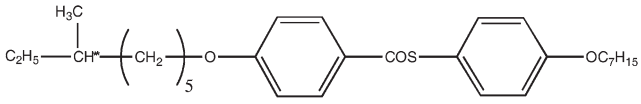

We used also mixtures of cholesteryl cinnamate with a non-chiral compound, synthesized by P. Keller, with phase sequence I–165°C–N–112°C–SmC–66°C–Cr, which we will call DOBCP.

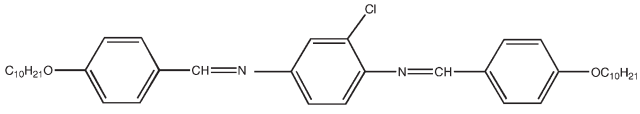

For the study of the SmC phase of materials exhibiting the N–SmC transition, the cells were filled with DOBCP. According to thickness we examined four classes of samples: (1) very thin samples of thickness $2\,\mu m < D < 4\,\mu m$ and perhaps lower; (2) thin samples with $5\,\mu m < D < 10\,\mu m$; (3) medium samples with $11\,\mu m < D < 15\,\mu m$; and (4) thick samples of thickness $20\,\mu m < D < 30\,\mu m$. The observations reveal the differences in layer structures in thin and thick samples; therefore, in the following, observations, discussion and an attempt at interpretation will be described separately for sample of different thickness. The aligning layers used were either SiO evaporated with an incidence angle of 60°, or polytetrafluoroethylene (PTFE) deposited by sliding a piece of this polymer on the glass plates at $1\,mm\,s^{-1}$, under a pressure of 10^6 Pa at 280°C. Both of these aligning layers are known to give planar alignment for nematic liquid crystals and a little more complex alignment (but approximately planar) for smectic liquid crystals. The smectic layer orientations inside the samples were investigated by X ray diffraction, for mixtures at room temperature only, with a four circles goniometer. The X ray source was an 18 kW rotating anode generator giving CuK_α radiation selected by a planar graphite monochromator. The diameter of the X-ray beam was about $1\,mm^2$. For X-ray experiments the cells were built with cover glasses (170 μm) which were thinned to about 50 μm using hydrofluoric acid.

3. Texture observations and discussion

3.1. *Very thin samples ($2\,\mu m < D < 4\,\mu m$)*

3.1.1. Observations. After the transition from the chiral nematic phase to the chiral smectic C phase a texture of twin domains appears, generally of a rectangular cross-section. Using the polarizing microscope, with crossed polarizers, the optical contrast of twin-like domains in thin samples was studied. This difference is increased in layers which are symmetrical with respect to the plane of the horizontal chevron interface. The chevron interface, by analogy with solids called a coherent wall [9], is usually perpendicular to the glass plates, or slightly inclined. The tilt of the smectic layers is seen in figures 1 (*a*) and 1 (*b*) showing the interface between the N* phase (as the sample thickness is about 2 μm, the N* helix is unwound) and the SmC* phase in a sample of ZLI 3079. The coherent wall, seen on the pictures as the line connecting two neighbouring domains (arrow 1), is parallel to the anchoring direction. The phase interface (arrow 2) copies the layer direction on each side of the coherent wall. This line gives the direction of the intersection of the layers with the surfaces. There are also shadows (arrow 3), perpendicular to the phase interface and therefore to the layers. They are visible in almost all the samples, and so indicate the projection on the surface of the normal to the layers. Extinction of the domains is reached when the local optical axis is parallel to one of the crossed polarizers. A rotation of about 14° leads from the extinction in figure 1 (*a*) to that of figure 1 (*b*).

When the SmC* phase is established in the sample, well defined, nearly rectangular, twin-like domains are observed as in figure 2. They are elongated, generally in the rubbing direction, so the coherent wall is longer than the incoherent wall. Sometimes the twin-like domain has a more complex shape which can be composed of a few rectangular domains as in figure 3. Parallelogram shapes are also possible, with coherent walls still in the rubbing direction. Figures 4 (*a–c*) show that in ZLI 3079 the optical contrast of a coherent wall is very sharp (arrow 1), indicating that the wall is perpendicular to the glass plates (or very slightly inclined). This also means that in very thin samples the walls are really planar objects going through the whole sample thickness. Like the wall, the smectic layers are probably perpendicular to the sample surfaces or

Downloaded At: 15:54 25 January 2011

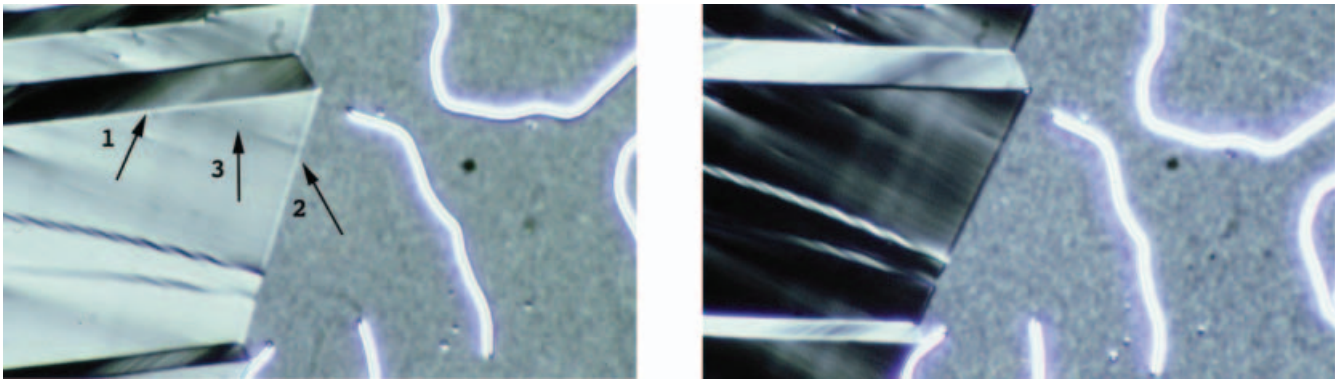

(*a*) (*b*)

Figure 1. Interface between N* phase and SmC* phase: ZLI 3079, SiO anchoring (2–4 μm). The coherent wall is seen as the line connecting two neighbouring domains: the phase interface is along the smectic layer directions. Between crossed polarizers, extinction in (*b*) is reached from (*a*) by a rotation of 14° (frame scale: $0.26 \times 0.4\,mm^2$).

slightly tilted. The incoherent wall is thicker and less straight (arrow 2). These pictures also show that, between crossed polarizers, when the anchoring direction is parallel to one of them, the colour and the illumination are the same on both sides of the walls, figure 4 (*a*). Turning the cell in its plane successively darkens each side in a total rotation of 14°, photos figures 4 (*b*, *c*). With a high magnification, figure 5 shows, for a mixture (6% cholesterol cinnamate in DOBCP), the coherent wall as a very thin line, both domains having the same illumination, figure 5 (*a*), when it is parallel to the polarizer. A rotation of 4° to the left gives the extinction of one domain, figure 5 (*b*), and a rotation of 4° to the right gives the extinction of the neighbouring domain, figure 5 (*c*).

Figures 6 (*a–c*) show the same situation with the non chiral compound, DOBCP, for which the total rotation is 7°. The domain shape is a little different from the SmC* case. Figure 6 (*d*) shows the walls closing the domain, observed without analyser. Coherent and incoherent walls have a different appearance: the coherent wall (arrow 1) is very sharp but shorter than in the previous case and the incoherent wall (arrow 2) is well defined, thick but longer than in the SmC* case. Some parts of the incoherent wall are parallel to the smectic layer direction (arrow 3); a single domain is less elongated than in the SmC* case.

X ray angular scans could not be obtained with these very thin cells, because the diffracted intensity was too low.

3.1.2. Discussion. The possibility of distinguishing twin-like domains from the surrounding structures by optical contrast is related to a small difference between the anchoring direction (SiO) or the sliding direction (PTFE) and the local optical axis. The average molecular direction, in the smectic layers, is parallel to the anchoring direction. But the direction of the core of the molecule, related to the optical axis, and thus to the extinction, is a little different. Figure 7 gives a

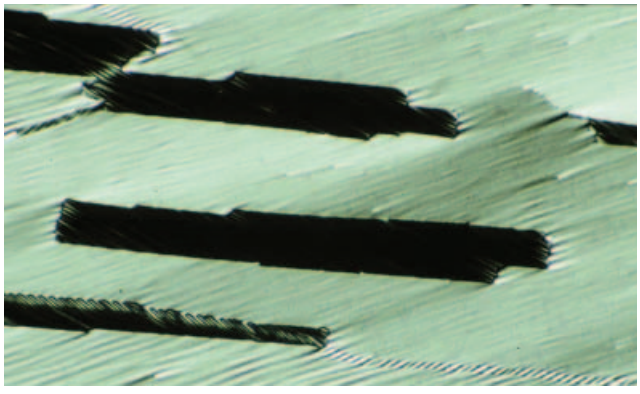

Figure 2. Twin-like domains, SiO aligning layer, ZLI 3079, 1.2 μm (frame scale: $0.26 \times 0.4\,mm^2$).

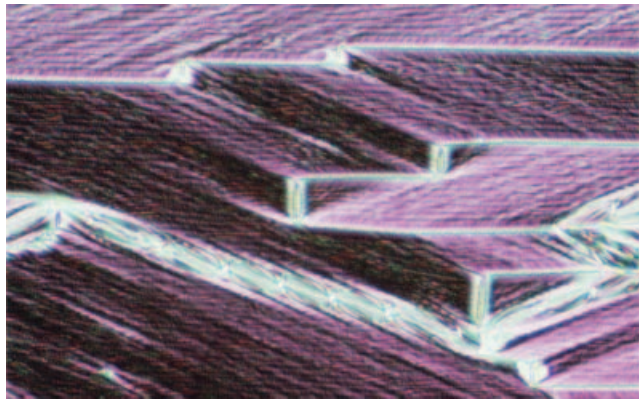

Figure 3. Domains with a coherent wall broken by incoherent walls (frame scale: $0.26 \times 0.4\,mm^2$).

Downloaded At: 15:54 25 January 2011

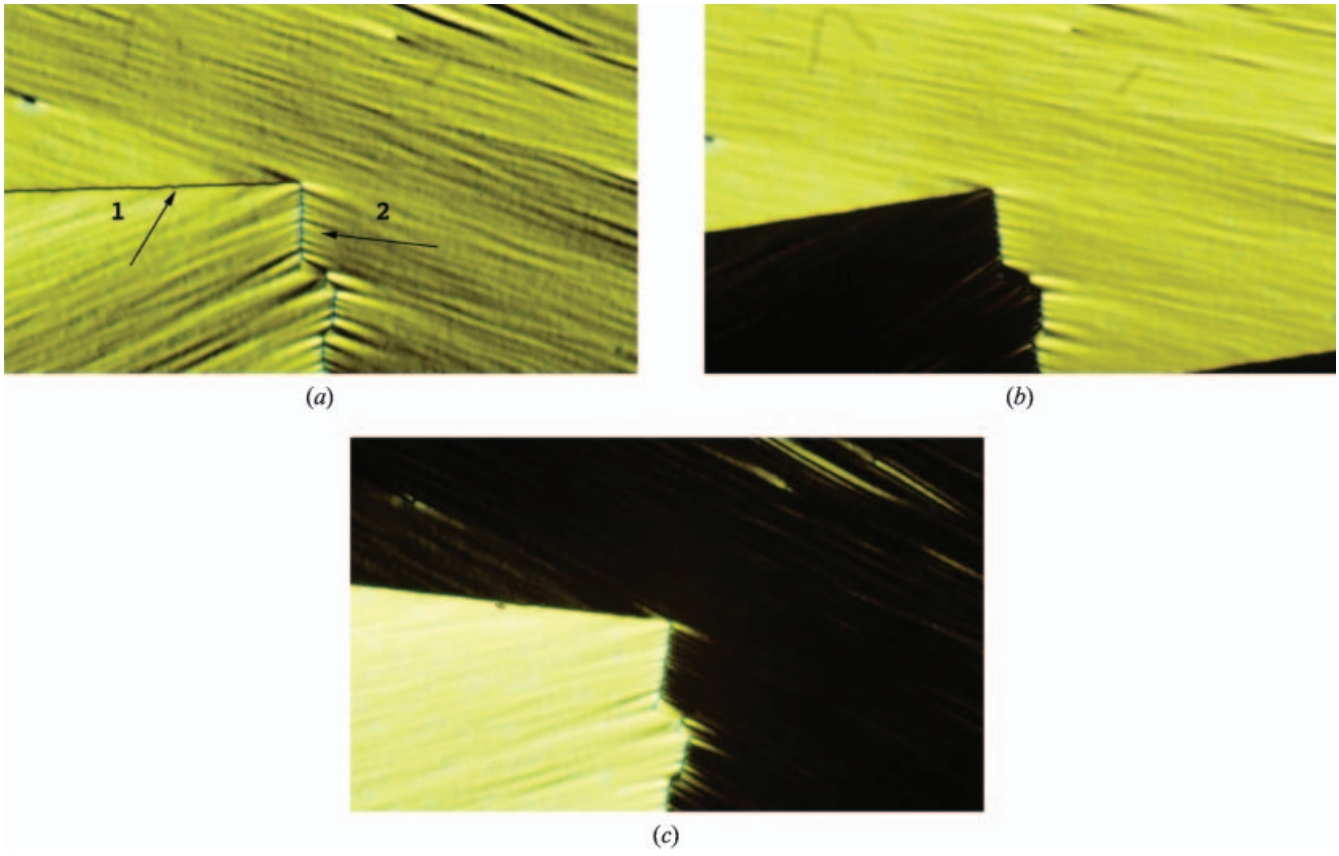

Figure 4. Coherent and incoherent walls in the same sample as in figure 2. (*a*) Anchoring parallel to the polarizer; extinction in (*c*) reached by a rotation of 14° starting from (*b*) (frame scale: $0.26 \times 0.4\,\mathrm{mm}^2$).

Downloaded At: 15:54 25 January 2011

representation of the molecular anchoring on each side of the coherent wall. The texture indicates that the layers are perpendicular to the surface (or a little tilted), every domain separated from its neighbour by a coherent wall which appears like a planar defect. Figure 8 is a model for the organization of the layers in domains of thicknesses illustrated in figures 2, 3, 4, 5. Figure 8 (*a*) is a sketch of figure 2, with two coherent walls, an incoherent one, and depicting the directions of the layers on both sides of each wall. Figure 8 (*b*) is a 3D representation of the directions of the layers and of the walls.

If an X-ray scan could give a measurable diffracted intensity, such a structure should give at $\chi=0°$ no intensity, whatever the value of θ, at $\chi=+30°$ one maximum at $\theta=0°$. But we recall that the total intensity for this thickness is too low to be measured.

3.2. *Thin samples ($5\,\mu m<D<10\,\mu m$)*

3.2.1. Observations. Generally in this case the limits of twin domains run from one side of the cell to the other, along the anchoring direction, with almost no incoherent wall closing the domains, as in figures 9 (*a*) and 9 (*b*). The domains are now parallel elongated bands. The domains are separated by bright stripes (arrow 1) as in figure 9 (*a*), with however some thin walls (arrow 2). More often, as in Figure 9 (*b*), stripes (arrow 1) alternate with thin walls (arrow 2). In both cases some straight bright lines (arrow 3) run between the stripes or between the stripes and the walls, at an angle of about $\pm 30°$ with the walls.

With slowly increasing thickness, walls and stripes become decorated by focal conics. The first visible ones (in relation to thickness) appear as hyperbola decorating the wall between two stripes (figure 10). It is known that the associated conics are ellipses, located in the plane of the walls, perpendicular to the picture plane. The ellipses are seen in the pictures as broken segments joining the foci of the hyperbola in figure 11, with uncrossed polarizers. The branches of the hyperbola are at an angle of about 40° to the anchoring direction. We will call this texture the 'hyperbola texture'.

In some locations of the same cell, as illustrated by figure 12, besides the hyperbola (arrow 1), in the plane of the figure, ellipses (arrow 2) start from the stripes in the same plane. The associated conics are known to be

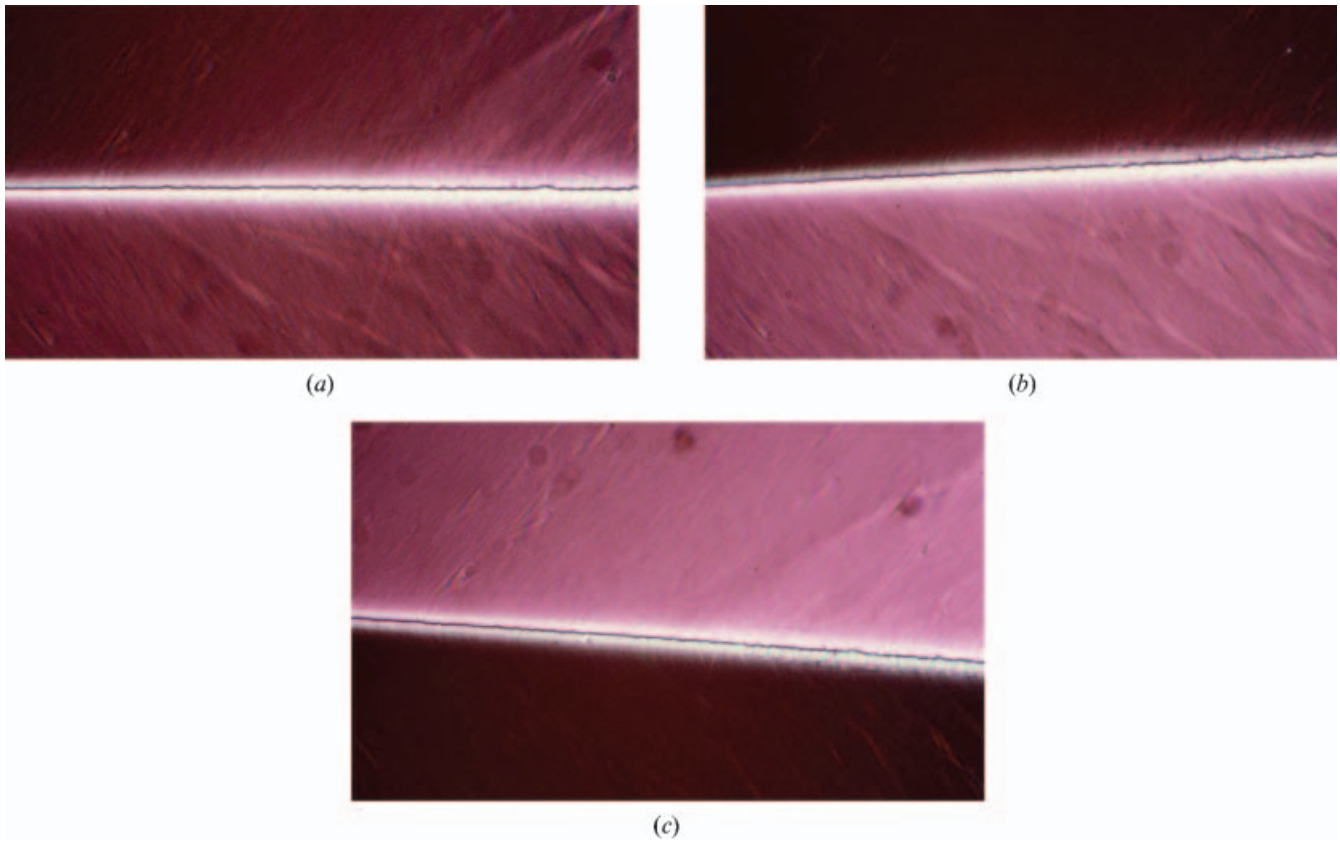

Figure 5. A coherent wall: (*a*) the wall is parallel to the polarizer crossed with the analyser. Rotation of 8° between (*b*) and (*c*), 6% cholesteryl cinnamate in DOBCP, SiO anchoring (frame scale: $0.18 \times 0.27\,mm^2$).

Downloaded At: 15:54 25 January 2011

hyperbola located in planes perpendicular to the plane of the ellipses. These hyperbolas can be seen as short straight lines (arrow 3) at one of the two tips of the ellipses. They have the same direction as the branches of the hyperbola arising from the coherent wall.

3.2.2. X ray experiments. The X-ray experiments were performed with a goniometer using two possible rotations (figure 13). At the start of the experiment the plane of the sample is parallel to (Ox, Oz). Oy is the direction of the X-ray beam and Oz the direction of the anchoring, A. The angle χ describes the rotation around Oy, $\chi=0°$ means that the anchoring direction is parallel to Oz. The angle θ describes the rotation around Ox, $\theta=0°$ means that the sample is perpendicular to the beam. The scan is made rotating the sample around Ox.

The angular scans for the Chisso compound in a cell of 7 μm thickness are given in figures 14 (*a*, *b*). The θ-scan, for $\chi=0°$, has two maxima at $\theta=-41.5°$ and $\theta=+36.5°$, and a non-zero intensity at $\theta=0°$, figure 14 (*a*). After a rotation of $\chi=\pm 30°$, the θ-scans present two narrow maxima at $\theta=-27°$ and $\theta=+26°$, and a wider and smaller one at $\theta=0°$ figure 14 (*b*) (we give only the scan for $\chi=+30°$, as the scan for $\chi=-30°$ is similar).

For this range of thickness there is no evident difference in the texture and in the X ray angular scans between samples prepared with PTFE and with SiO.

3.2.3. Discussion. In the 'hyperbola texture' the ellipses form a planar object, which was a coherent wall in very thin samples and is now more structured. This texture exhibits a focal conic wall, as described by Kléman and Lavrentovich [11]. Close to the wall the focal conics avoid an abrupt change in the layer orientation which is present in chevrons. In our observations, this layer orientation change is replaced by a bend. Far from this wall, the hyperbola is perpendicular to the intersection of the smectic layers with the glass plates. These smectic layers can be vertical, tilted or forming a 'vertical chevron' in relation with the thickness. We must emphasize that the size of the domain 'seen' by the X-ray beam (about $1\,mm^2$), is larger than the size of the domain seen by the light beam ($0.013–0.05\,mm^2$). Therefore it is not possible to show a scan corresponding exactly to one photomicrograph frame.

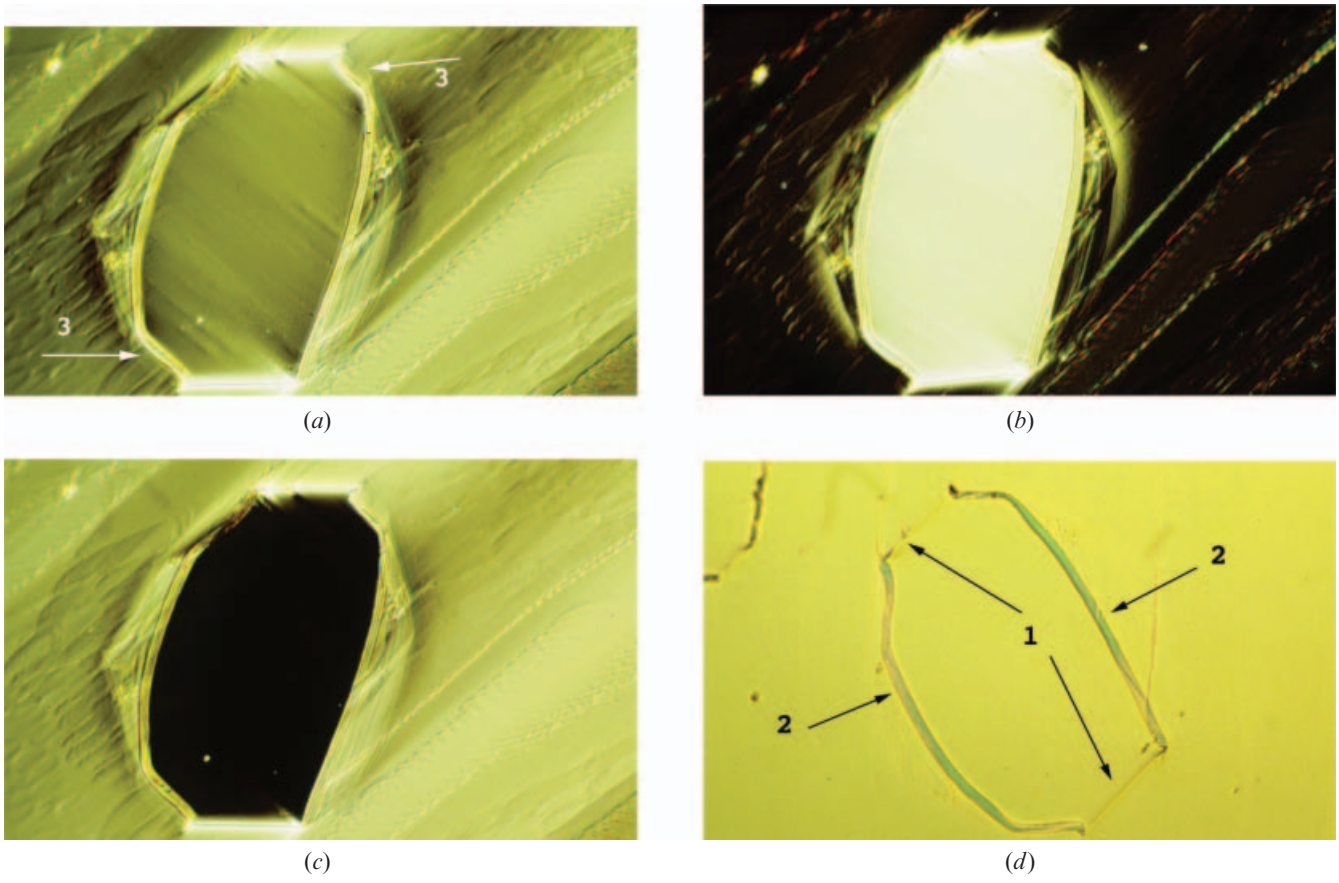

Figure 6. A domain surrounded by coherent and incoherent walls in non-chiral smectic C. DOBCP, 2 μm, SiO anchoring. (*a*) Anchoring parallel to the polarizer. Rotation of 7° between (*b*) and (*c*). (*d*) Without polarizer (picture scale: $0.26 \times 0.4\,\text{mm}^2$).

The θ-scan, at $\chi=0°$, figure 14 (*a*), indicates that there are two directions of smectic layers which intercept the boundary surfaces along the normal to the anchoring direction, tilted in relation with the normal to the surfaces and having slightly different tilt angles. This can be given by the smectic layers which surround the ellipses located in the plane which was the coherent wall, figures 15 (*a*, *b*). The non-zero intensity at $\theta=0°$ may be attributed to some parts of the layers belonging to the focal conics and also, perhaps, to layers belonging to the stripes.

In the θ-scan, at $\chi=+30°$, figure 14 (*b*), the two narrow maxima at $\theta=-27°$ and $\theta=+26°$ indicate that there is a 'vertical chevron', whose layers intercept the surfaces along the normal to the branches of the hyperbola in the 'hyperbola texture'. The wide maximum at $\theta=0°$ shows that some of these chevrons have no fracture in the middle but a weak bend. In figure 10 no ellipse is located in the plane parallel to the surfaces, the corresponding θ-scan would not have a maximum at $\theta=0°$, but we have no scan relating exactly to this micrograph. In figure 12 some ellipses are located in the

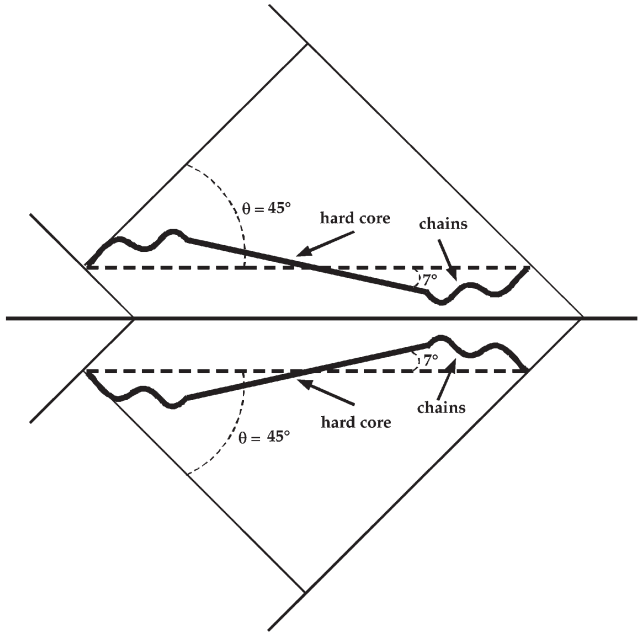

Figure 7. Molecular anchoring on both sides of the coherent wall.

Downloaded At: 15:54 25 January 2011

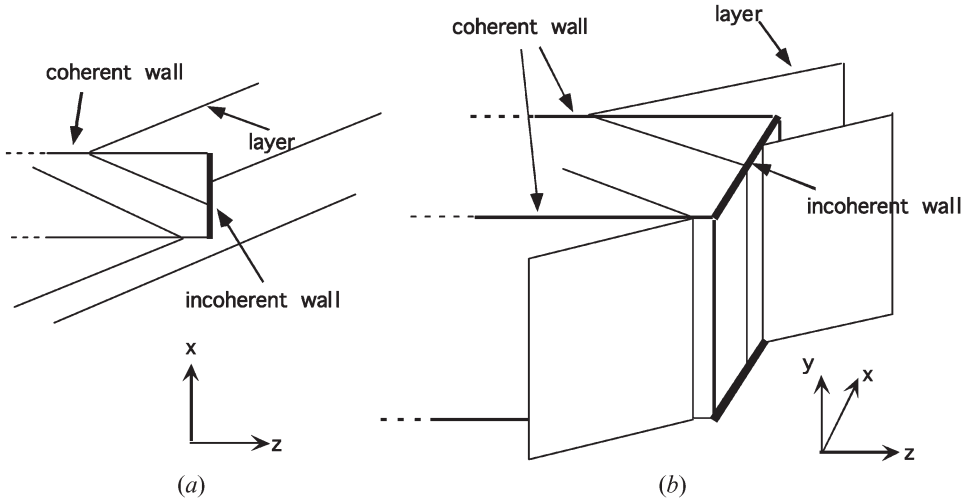

Figure 8. Model of the organization of layers related to the textures of very thin samples, horizontal chevron, illustrated by figures 2,3,4,5.

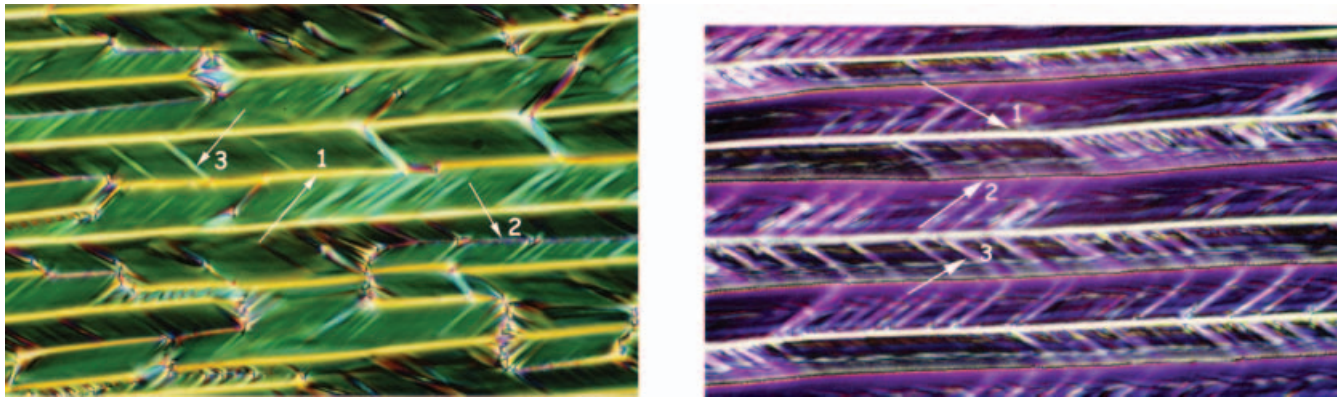

Figure 9. (*a*) Typical coherent walls (2); stripes parallel to the anchoring direction (1). Chisso 2004, PTFE anchoring, 7 μm thick. (*b*) Thin walls (2) alternate with stripes (1); bright straight lines (3) are at an angle of $\pm 30^\circ$ with the straight lines. Chisso 2004, PTFE anchoring, 10 μm thick (frame scale: $0.18 \times 0.27\,\mathrm{mm}^2$).

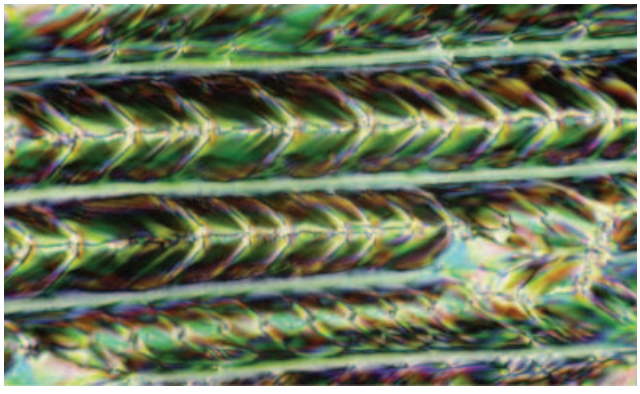

Figure 10. 'Hyperbola texture.' Chisso 2004, PTFE anchoring, 10 μm thick (frame scale: $0.09 \times 0.14\,\mathrm{mm}^2$).

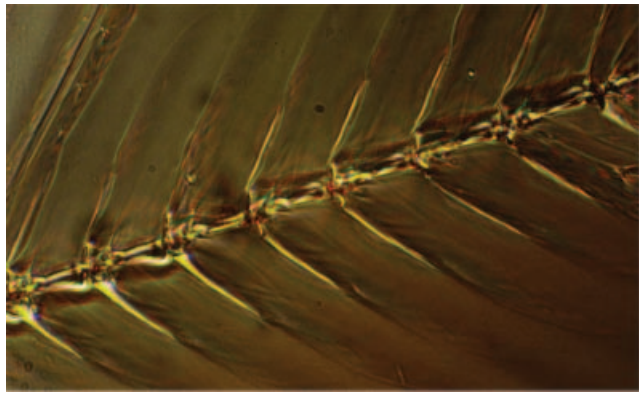

Figure 11. The 'hyperbola texture' seen without polarizer (frame scale: $0.26 \times 0.4\,\mathrm{mm}^2$).

Downloaded At: 15:54 25 January 2011

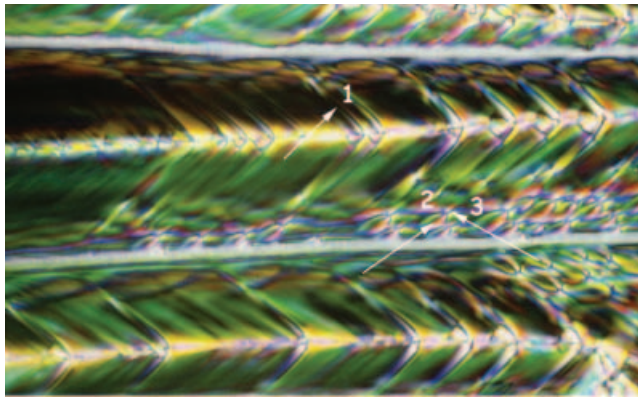

Figure 12. 'Hyperbola texture' (1) decorated by ellipses (2) with the associated hyperbola seen as a small straight line (3). Chisso 2004, PTFE anchoring, 10 µm thick (frame scale: $0.09 \times 0.14\,mm^2$).

plane parallel to the surfaces; the θ-scan of figure 14 (*b*) illustrates this texture. The two maxima indicate the direction of the smectic layers normal to the branches of the hyperbola at the tip of the ellipses located in the plane parallel to the surfaces. The existence of this chevron indicates a slight dependence of the tilt molecular tilt angle on temperature in the SmC* phase. This is probably because the compound is a mixture.

The θ-scan at $\chi = -30^\circ$, similar to the previous one at $\chi = +30^\circ$, indicates a situation symmetrical in relation to the coherent wall. Figure 16 is a sketch of the texture in these cases. In figure 16 (*a*), corresponding to figures 9 (*a*, *b*), with no focal conics, some straight bright lines

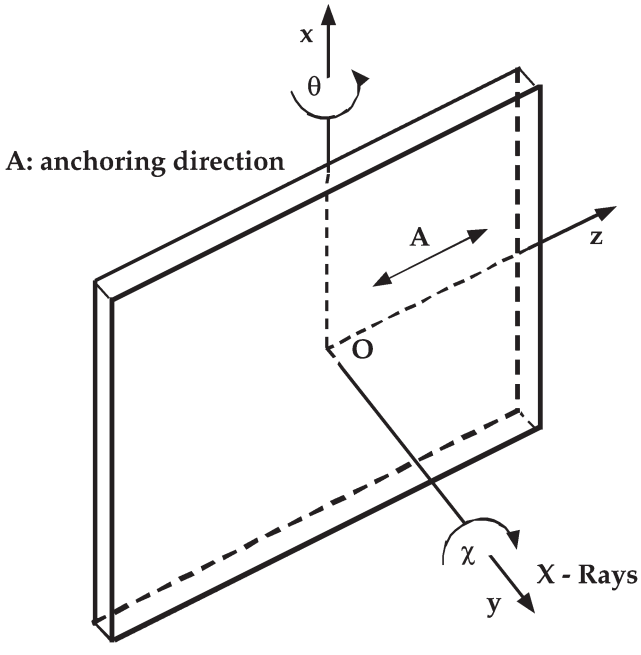

Figure 13. Reference axis in relation to the sample and to the rotations in X-ray diffraction.

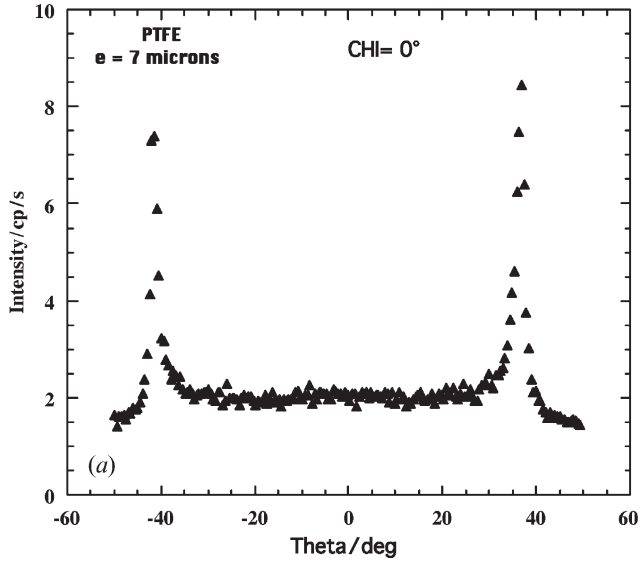

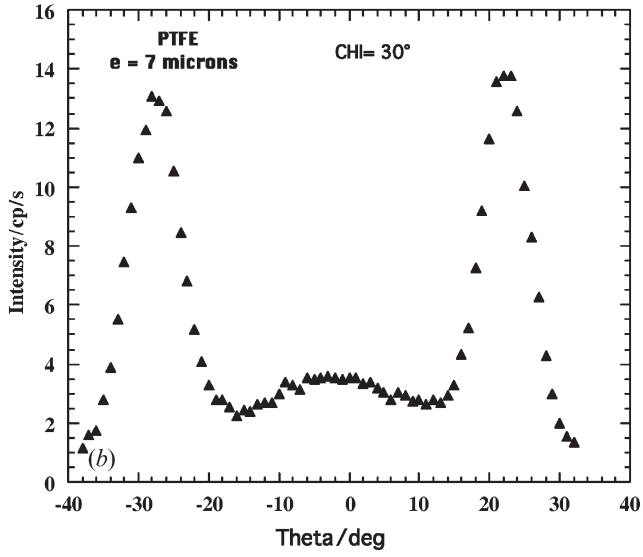

Figure 14. X-ray spectra: (*a*) $\chi = 0^\circ$; (*b*) $\chi = 30^\circ$. Chisso 2004, PTFE anchoring, 7 µm thick.

proceed from the stripes toward the walls, at an angle of $\pm 30^\circ$. In figure 16 (*b*) corresponding to figure 10, the walls are becoming decorated with linear arrays of hyperbola; and in figure 16 (*c*), corresponding to figure 12, ellipses arise, in opposite directions, from one stripe, along the branches of the hyperbola located in the picture plane. On these figures are indicated the possible contribution of some elements of the texture to the maxima detected on the X-rays scans. Figure 17 illustrates a model for the organization of the smectic layers in this domain of thickness. In figure 17 (*a*), corresponding to figure 16 (*a*), a vertical chevron is added to the horizontal one; it is a model for figure 9 (*b*). Figure 17 (*b*), corresponding to figure 16 (*b*)

Downloaded At: 15:54 25 January 2011

Downloaded At: 15:54 25 January 2011

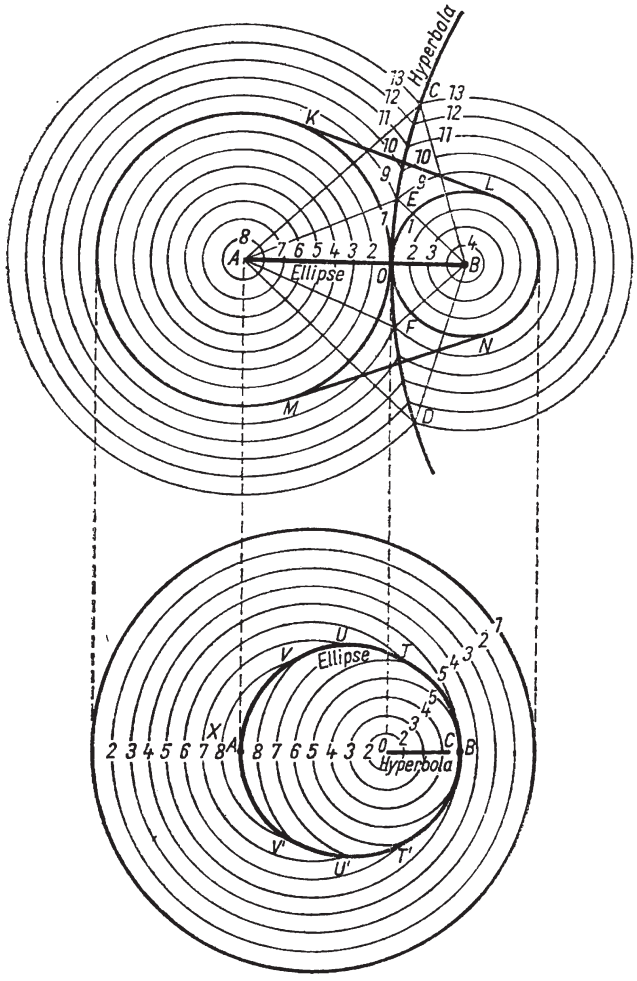

(*a*)

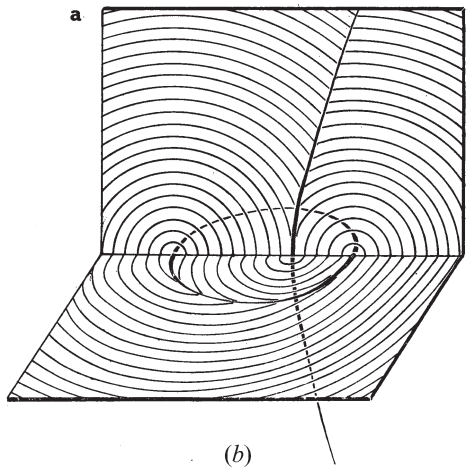

(*b*)

Figure 15. (*a*) Dupin cyclide after *Crystals and the Polarising Microscope* (N.H. Hartshorne, A. Stuart, Edward Arnold Publishers, 1970). (*b*) Ellipse and associated hyperbola after Y., Bouligand *J. Physique,* **33**, 525, 1972.

is a model for figure 10, in which the coherent wall is replaced by a wall of ellipses with hyperbola in the x z-plane. In some places the vertical chevron can be replaced by a bend of the layers, proved by the small ellipses, and by the maximum at $\chi=+30^\circ$, $\theta=0^\circ$. The model drawn in figure 17 (*c*) is related to figure 16 (*c*). In such a case the smectic layers in the stripes are normal to the anchoring direction and to the glasses, they could also form a curved surface contributing to the non-zero intensity at $\chi=0^\circ$, $\theta=0^\circ$.

3.3. *Medium samples (11 μm<D<15 μm)*

3.3.1. Observations. We have emphasized that, for thin cells, elongated domains are generally separated alternately by stripes and walls, and sometimes only by stripes. In cells of medium thickness, on the contrary, there are almost no walls but only stripes. At the same time the 'hyperbola texture' disappears and is replaced by the 'ellipse texture'. Figure 18, in a Chisso 2004 sample with PTFE anchoring (10 μm), a mixture of various textures is a good example of the change from one to the other. The area I is similar to figure 9 (*b*), and area II is similar to figure 10. In area III small ellipses and the associated hyperbolas (arrows 1 and 2) arise from two neighbouring stripes at the same angle, pointing in opposite directions. Comparing area II with area III, it may be noted that the coherent wall decorated by the hyperbola is replaced by a stripe (arrow 3) and the branches of the hyperbola replaced by new ellipses (arrow 2) whose tips point towards the tips of the first ellipses. Above 11 μm the 'ellipse texture', occupies the whole field. The opposite ellipses, indicated by arrows 1 and 2 in figure 19, in a ZLI 3079 sample with SiO anchoring (13 μm) between two neighbouring stripes (arrow 3) are separated by a complex texture that appears as a helix, arrow 4. There are no more thin walls. In the same sample the ellipses decorating the stripes are shown under high magnification, in figure 20.

3.3.2. X-ray experiments. Figures 21 (*a*, *b*) give the X-ray scans for the compound Chisso 2004, with a cell thickness of 11 μm and PTFE treatment. They are the θ-scans with, respectively, $\chi=0^\circ$ and $\chi=+37^\circ$. The θ-scan, for $\chi=0^\circ$ has two narrow maxima at $\theta=+39^\circ$ and $\theta=-39^\circ$, figure 21 (*a*). After a rotation of $\chi=\pm 37^\circ$, the θ-scans present two maxima at $\theta=-22^\circ$ and $\theta=+22^\circ$ and a higher one at $\theta=0^\circ$, figure 21 (*b*); the scan for $\chi=-37^\circ$ is similar.

3.3.3. Discussion. In this 'ellipse texture', the θ-scans with, respectively, $\chi=0^\circ$ and $\chi=+37^\circ$, show the layer orientations as a combination of vertical and horizontal

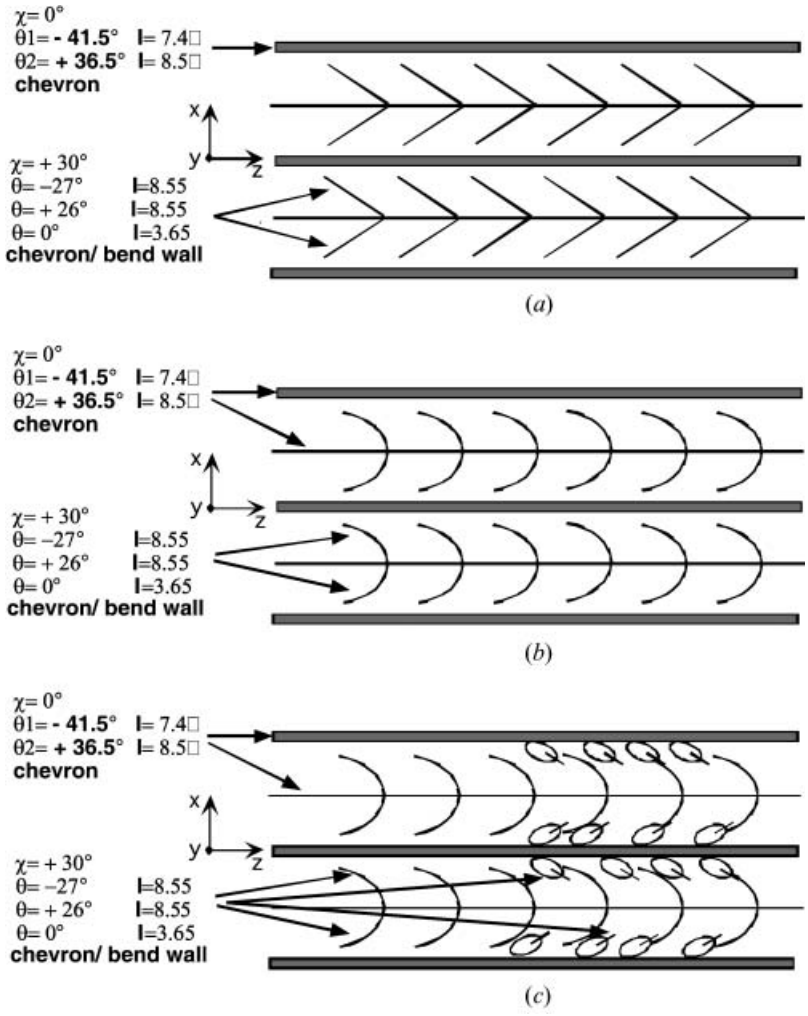

Figure 16. Sketch of the textures for thin samples and the possible contribution to the maxima in the X-ray scans: (*a*) for figure 6 (*b*), (*b*) for figure 10, (*c*) for figure 12.

chevrons. Figure 22 is a model of the texture in this domain of thicknesses, as seen in figure 19. We give the possible contribution of some elements of the texture to the maxima detected on the X-rays scans. Figure 23 is a possible representation of the layer organization relating to figures 19, 20 and 22. The wall of ellipses is replaced by a complex texture, which has the appearance of a helix. We are unable to propose a model of the layer organization for this texture. The high intensity at χ=+37° and θ=0°, proves that chevrons are essentially replaced by bend walls.

3.4. *Thick samples (20 μm<D<30 μm)*

From the optical point of view, the textures in thick samples are similar to those in samples of medium thickness. The number of focal conics increases in relation to the thickness. A new texture has also been observed, especially with SiO anchoring. We do not describe this texture which is far removed from twin-like domains.

The X-ray angular scans are quite similar to those presented for medium samples, with some variation in the angles where the maxima are located. Figures 24 (*a*, *b*) are scans for Chisso 2004 with cell thickness 28 μm and PTFE treatment. The θ-scan, for χ=0° shows two maxima, at θ=−40° and θ=+40°, indicating the same situation as in the previous cases. The θ-scan, for $\chi=\pm 36°$ has two maxima at θ=−22° and θ=+22°, but they have different intensities; a maximum for θ=0° is lower than in the previous case.

In this range of thickness the texture is increasingly complex, and interpretation, even with the help of the X-ray scans, is more difficult. However one comment

Downloaded At: 15:54 25 January 2011

Downloaded At: 15:54 25 January 2011

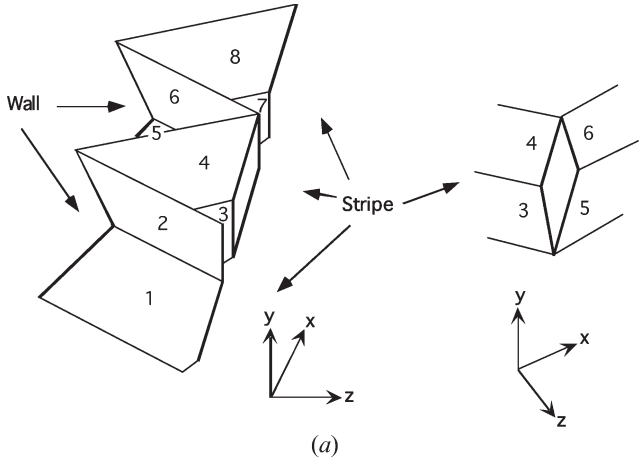

(*a*)

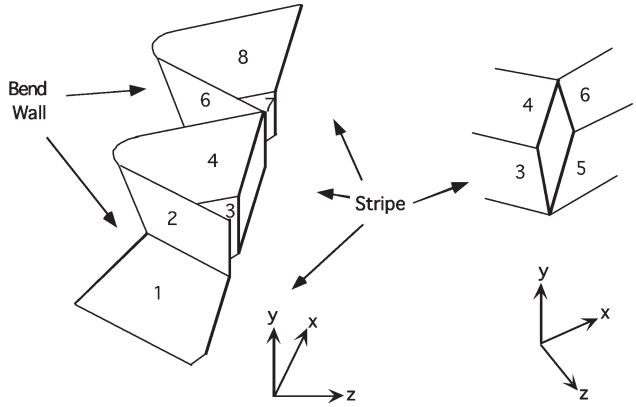

(*b*)

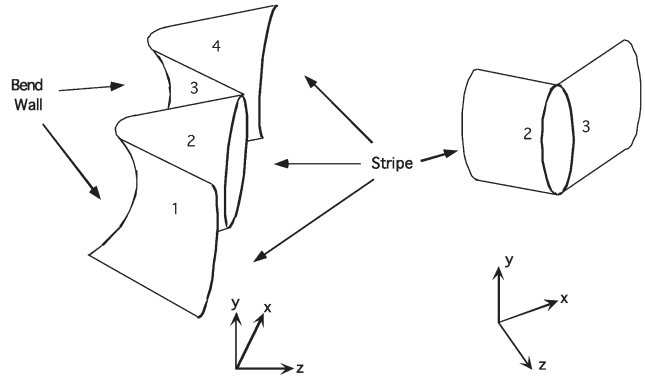

(*c*)

Figure 17. (*a*) Model of the organization of layers corresponding to the textures of thin samples sketched on figure 16 (*a*); a vertical chevron is added to the horizontal one of figure 8. (*b*) Model corresponding to the sketch of figure 16 (*b*). The horizontal chevron becomes a bend wall. (*c*) Model corresponding to the sketch of figure 16 (*c*). The vertical chevron becomes a bend wall.

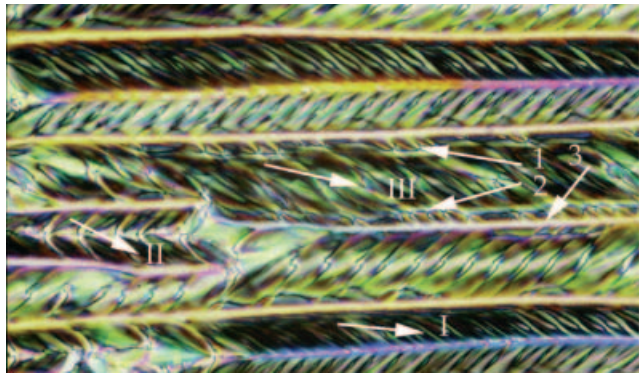

Figure 18. Mixed textures. I: similar to figure 7 (*b*). II: similar to figure 8 (*a*). III: ellipses in opposite directions (1 and 2). Chisso 2004, PTFE anchoring, 10 μm thick (frame scale: $0.18 \times 0.27\,\mathrm{mm}^2$).

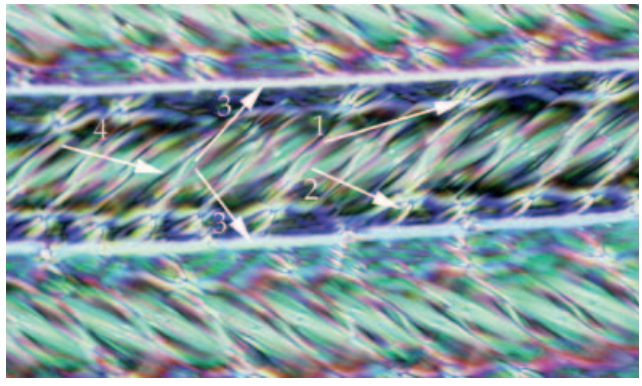

Figure 19. 'Ellipse texture': stripes (3), opposite ellipses (1 and 2). The observed texture resembles a kind of helix (4). ZLI 3079, SiO anchoring, about 13 μm thick (frame scale: $0.09 \times 0.14\,\mathrm{mm}^2$).

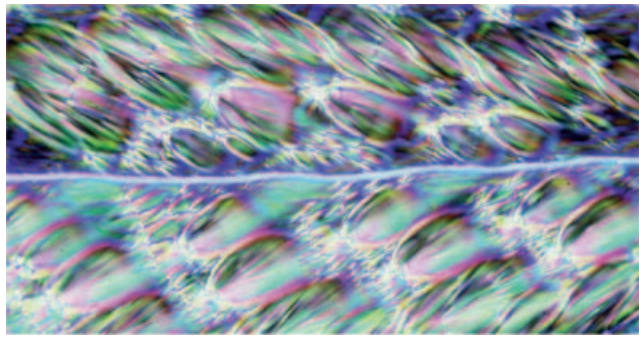

Figure 20. Ellipses starting from a stripe in opposite directions. ZLI 3079, SiO anchoring, about 13 μm thick (frame scale: $0.18 \times 0.27\,\mathrm{mm}^2$).

can be made: the θ-scans for $\chi = \pm 36^\circ$ show that there are essentially bend walls, the layers of which intercept the surfaces at $\pm 36^\circ$ to the aligning direction.

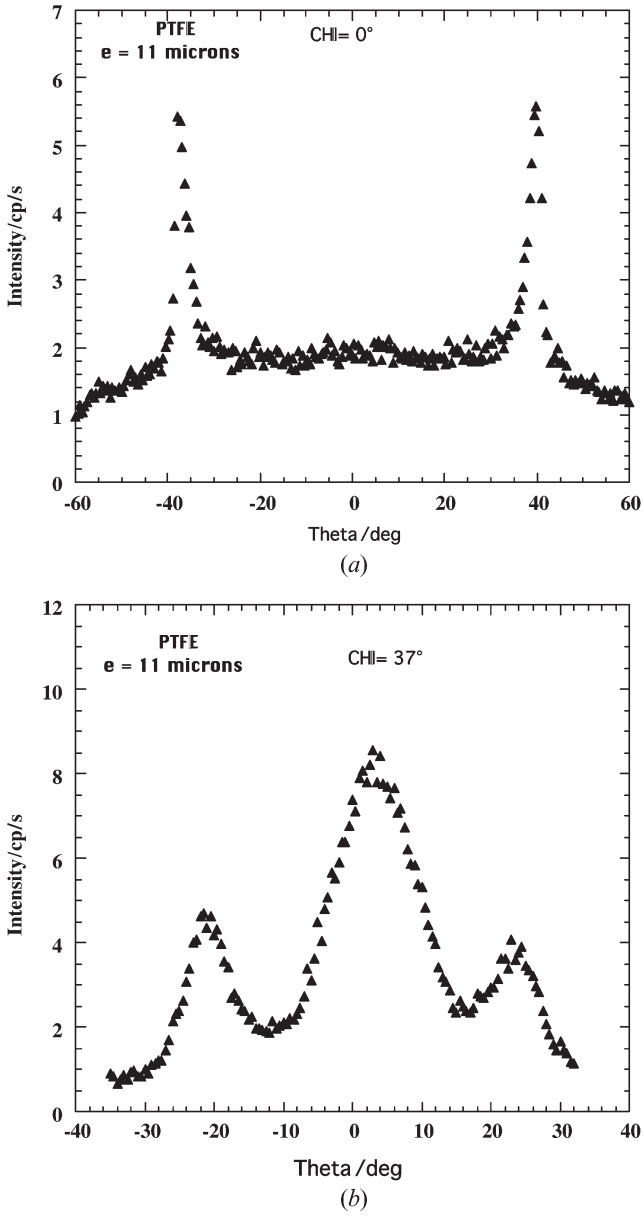

Figure 21. X-ray spectra: (*a*) $\chi=0^\circ$, (*b*) $\chi=37^\circ$. Chisso 2004, PTFE anchoring, 11 μm thick.

3.5. *Conclusions concerning the textures*

The discussions on organization of the layers in relation to the thickness of the samples, leads to the following conclusion: the coherent wall appears as a uniform planar defect normal or almost normal to the glass plates only for cells whose thickness is less than about 5 μm. When the thickness is about 5–10 μm, the coherent wall is replaced, in the 'hyperbola texture', by a plane of ellipses associated with hyperbolae located in a plane parallel to the surfaces. The plane is no longer a planar defect but a plane of linear defects, the ellipses. The incoherent wall is no longer present for domains of this thickness. When the thickness is about 11–15 μm, one can say that in the 'ellipse texture' the wall of ellipses does no longer exists; it is replaced by a very complex 3D defect, seen on the micrographs as a kind of helix.

Above 20 μm the texture is increasingly complex, with stripes and ellipses, proving the presence of bend walls in the organization of the layers. The numerical values give the order of the thicknesses but are imprecise.

3.6. *Influence of an electric field*

When a d.c. electric field is applied to the SmC* sample of ZLI 3079, molecular switching is observed, which is not followed by wall motions. This observation differs from [3] where domain wall motion under a d.c. electric field was reported in SmC* phases of 8OBE (+)-4-*n*-octyloxyphenyl 4-(2′-methylbutyl)biphenyl-4′-carboxylate). In [3] twin-like domains are removed by the wall motion driven by an applied d.c. electric field; but on examining the micrographs the pictures and graphs in [3], the cholesteric seems not to be unwound at the N*–SmC* transition, and smectic layers were formed in a twisted structure inducing a kind of artificial TGB_c structure. In our case, for the 2–3 μm thick ZLI 3079 sample, the only effect of a d.c. electric field up to of $40\,V\,\mu m^{-1}$ on the coherent walls, was to change the straight smooth line in the hyperbola structure. Change of domain shape was never observed in samples of non-chiral DOBCP or $C_9\,H_{19}$ under an applied d.c. field up to about $40\,V\,\mu m^{-1}$.

4. Theoretical description of twin domains in very thin samples

In this section an approximate elastic model of one rectangular twin-like domain observed in thin samples (see § 3.1) is constructed. The model will describe the layer deformation inside and outside the domain.

4.1. *An approximate elastic model of a rectangular twin domain*

Let the reference state of the SmC* be the system of non-deformed smectic layers parallel to the *xy*-plane with the layer normal parallel to the *z*-axis (figure 13). Sample surfaces are supposed to be perpendicular to the *y*-axis and therefore to smectic layers. The molecular orientation in smectic layers is described by the unit **t**-vector which is the orientation of the molecular projection onto the layer plane. The rotation of the

Downloaded At: 15:54 25 January 2011

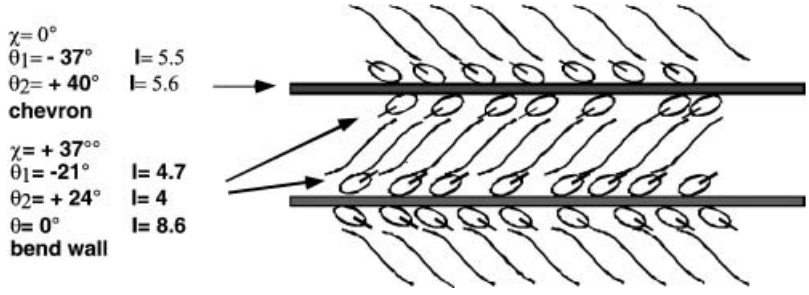

Figure 22. Sketch of the texture for medium samples and the possible contribution to the maxima in the X-ray scans for figures 19 and 20.

t-vector around the z-axis is characterized by an angle Φ. Then the **t**-vector can be defined as $\mathbf{t}=(\cos\Phi, \sin\Phi, 0)$. The elastic free energy of a SmC* for small gradients of the layer displacement u and for small angles Φ can be expressed by the approximation given in [12]:

$$f = \frac{A_{11}}{2}\left(\frac{\partial^2 u}{\partial x \partial y}\right)^2 + \frac{A_{12}}{2}\left(\frac{\partial^2 u}{\partial x^2}\right)^2 + \frac{A_{21}}{2}\left(\frac{\partial^2 u}{\partial y^2}\right)^2 + \frac{\bar{B}}{2}\left(\frac{\partial u}{\partial z}\right)^2 + \frac{B_1}{2}\left[\left(\frac{\partial \Phi}{\partial x}\right)^2 + \left(\frac{\partial \Phi}{\partial y}\right)^2\right] + \frac{B_3}{2}\left(-\frac{\partial \Phi}{\partial z} + q\right)^2 + B_{13}\left(\frac{\partial \Phi}{\partial z}\right)\left(\frac{\partial \Phi}{\partial x}\right) + C_1\left(\frac{\partial^2 u}{\partial x \partial y}\right)\left(\frac{\partial \Phi}{\partial x}\right) + C_2\left(\frac{\partial^2 u}{\partial y^2}\right)\left(\frac{\partial \Phi}{\partial y}\right). \quad (1)$$

Here the parameters A_{11}, A_{12}, and A_{21} are the elastic constants corresponding to a layer curvature deformation, $\bar{B}$ characterizes the layer compressibility, $B_1=B_2$, B_3 and B_{13} describe the **t**-vector rotation (which is supposed to be isotropic in the xy-plane) and the constants C_1 and C_2 determine the interaction between the layer deformation and the **t**-vector rotation. The parameter q is related to the helical pitch Z: $q=2\pi/Z$. In the following we take $B_{13}\approx 0$.

This elastic free energy will be used to construct the solution describing the rectangular twin-like domain schematically shown in figure 25. We use a method developed in [13] for the theoretical case of twin domain in smectic A (SmA). In [13] the twin domain was described by two separated edge dislocation walls. Each wall contains dislocations of the same sign but walls have the total dislocation Burgers vector of opposite sign. Dislocation walls correspond to so called incoherent walls of a twin domain. In the SmC* case we first find the solution describing the layer deformation corresponding to the observed layer structure in a twin domain, and then discuss the director orientation.

As the tilt angle θ is relatively high in SmC* materials with the phase sequence N*–SmC* (the commercial mixture ZLI 3079 in the SmC* phase has $\theta\sim 36^\circ$) smectic layers along a coherent twin boundary are inclined by an angle 2θ (figure 25). Then the incoherent twin boundary (tilt wall) which closes a twin domain is composed of edge dislocations situated at distances d. If the Burgers vector of an elementary dislocation is $b_o\approx a_o$ (a_o=the smectic layer thickness) their distance d can be expressed as $d\approx(b_o/2)\cot\theta$. As the dislocation core radius r_o can be estimated as $r_o\sim b_o/2$ [14] it can be seen that, for $\theta\sim 36^\circ$, $d\approx 1.4(b_o/2)<2r_o\approx b_o$, so the dislocation cores in the wall are overlapped. Therefore we now deal with the so-called melted grain boundary discussed by Dozov [15]. In this case the incoherent twin boundary can be modelled as the continuous distribution of edge dislocations with the density $1/d$ and with Burgers vectors $b_o\approx 2d\tan\theta$.

Suppose first that the twin domain is created in the whole sample thickness and that the interaction of edge dislocations terminating at sample surfaces with these surfaces can be neglected. Then we can describe an edge dislocation parallel to the y-axis (oriented along the sample thickness) by the well known solution [16, 17]:

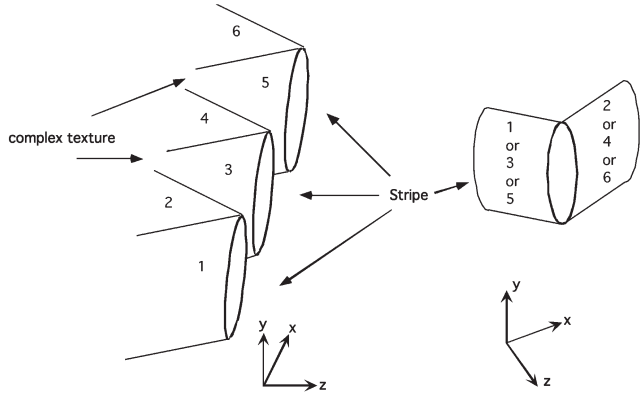

Figure 23. Model of the organization of layers for the textures of medium samples, related to the sketch of figure 22. There are stripes but no walls of ellipses.

Downloaded At: 15:54 25 January 2011

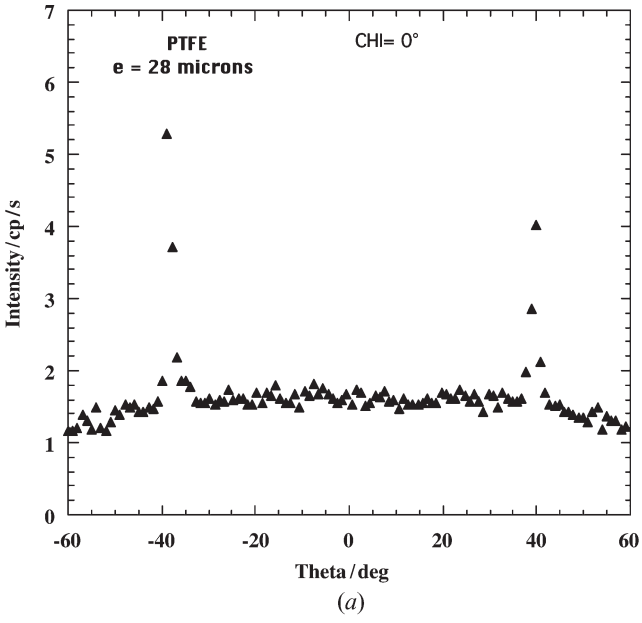

(*a*)

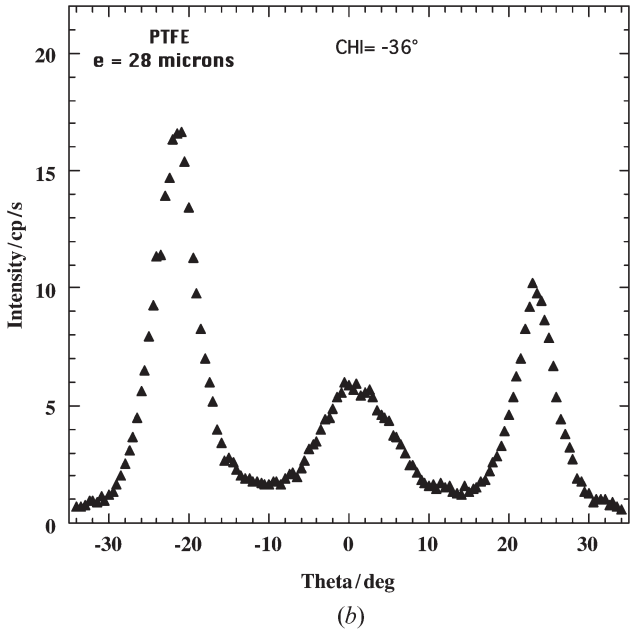

(*b*)

Figure 24. X-ray spectra: (*a*) $\chi=0^\circ$, (*b*) $\chi=-36^\circ$. Chisso 2004, PTFE anchoring, 28 μm thick.

$$u_\mathrm{d} = -(b_\mathrm{o}/4)\,\mathrm{sgn}\,(z)\left[1+\mathrm{erf}\,(x/2(\lambda|z|)^{1/2}\right],$$
$$\text{with } \lambda = A_{12}/\overline{B}.$$

The solution u_d satisfies the equation

$$\lambda\frac{\partial^4 u_\mathrm{d}}{\partial x^4} - \frac{\partial^2 u_\mathrm{d}}{\partial z^2} = 0 \qquad (2)$$

for all x and z with the exception of the point [0, 0]. Now, similarly as in [13], the solution describing the semi-infinite incoherent wall lying along the x-axis and

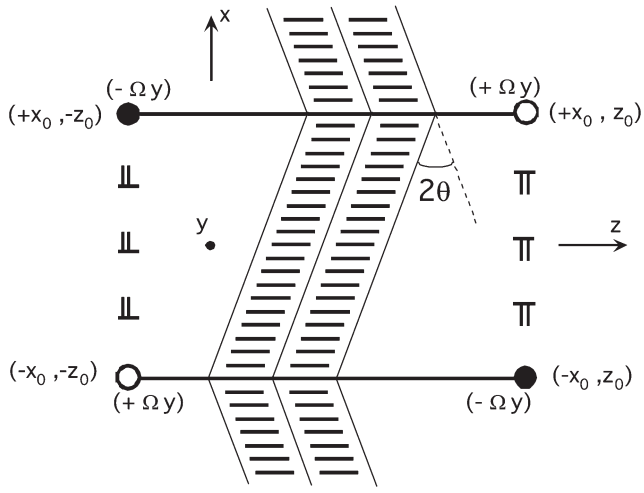

Figure 25. Schematic representation of a twin-like domain, symbols (●) and (o) represent wedge disclinations, (⊥) denotes edge dislocations.

starting at the point x_o will be calculated as the continuous dislocation distribution with the density $1/d$:

$$u(x,z) = \frac{1}{d}\int_{x_o}^{\infty} u_\mathrm{d}(x-x',z)\,\mathrm{d}x' = -\frac{\tan\theta}{2}\,\mathrm{sgn}\,(z)$$
$$\left\{(x-x_o)+2(\lambda|z|/\pi)^{1/2}\exp\left[-(x-x_o)^2\Big/4\lambda|z|\right]\right. \qquad (3)$$
$$\left.+(x-x_o)\,\mathrm{erf}\left[\frac{(x-x_o)}{2(\lambda|z|)^{1/2}}\right]\right\}$$

The error function $\mathrm{erf}\,(x)$ is defined as $\mathrm{erf}\,(x) = \frac{2}{\sqrt{\pi}}\int_0^x \exp\left(-t^2\right)\mathrm{d}t$.

The solution (3) is equivalent to the solution of a wedge disclination in the system of smectic layers characterized by the Frank vector of rotation $\boldsymbol{\Omega}=(0,\ -2\theta,\ 0)$ [13]. Using the expression (3) the total elastic solution of a twin domain of a rectangular cross-section can be constructed from solutions of two finite incoherent walls of length $2x_\mathrm{o}$ situated at $\pm z_\mathrm{o}$. As each incoherent wall of a finite length is elastically equivalent to a pair of edge disclinations of opposite signs the twin domain can be described by a disclination quadrupole with $(-\Omega_y)$-disclination at the point $[-x_\mathrm{o},\ z_\mathrm{o}]$, $(+\Omega_y)$-disclination at $[x_\mathrm{o},\ z_\mathrm{o}]$, $(-\Omega_y)$-disclination at $[x_\mathrm{o},\ -z_\mathrm{o}]$, and $(+\Omega_y)$-disclination at $[-x_\mathrm{o},\ -z_\mathrm{o}]$ (figure 25). This disclination quadrupole leads to the layer inclination inside a twin domain by an angle $\Omega_y \approx -2\theta$ with respect to smectic layers outside a domain. It should be noted, however, that such an elastic solution is valid away from coherent and incoherent walls because we work with the linear elasticity approximation. It is the so-called optical scale limit, discussed by Kléman [11]. In this limit the

Downloaded At: 15:54 25 January 2011

deformation within walls, i.e. their proper energy, is not taken into account and walls are taken as walls of the layer inclination changes. This approach is analogous to the similar problem of a twin of rectangular cross-section in a linear elastic media [18].

As the rectangular twin domain is composed of four wedge disclinations its elastic energy E_Q (per unit length in the y-direction) is the sum of four disclination self-energies E_s and corresponding interaction energies E_I. In [13] the energies E_s and E_I were determined as follow:

$$E_s = \overline{B}\lambda\left[\tan\left(\Omega_y/2\right)\right]^2 R/\pi \tag{4}$$

and

$$E_I = \frac{2\overline{B}\lambda}{\pi}\tan\left(\Omega_y^I/2\right)\tan\left(\Omega_y^{II}/2\right)\{R - \frac{\pi|x_2-x_1|}{2}\left[1+\operatorname{erf}\left(|x_2-x_1|/2(\lambda|z_2-z_1|)^{1/2}\right)\right] - (\pi\lambda|z_2-z_1|)^{1/2}\exp\left[-(x_2-x_1)^2/4\lambda|z_2-z_1|\right]\} \tag{5}$$

which is the interaction energy between two wedge disclinations Ω_y^I and Ω_y^{II} situated at points $[x_1, z_1]$ and $[x_2, z_2]$. The parameter R is the sample dimension in the xz-plane. By using expressions (4) and (5) the energy E_Q can be written as:

$$E_Q = 4\overline{B}\lambda\left(\tan\frac{\Omega_y}{2}\right)^2\left\{x_o\left[1-\operatorname{erf}\left(\frac{x_o}{(2\lambda|z_o|)^{1/2}}\right)\right] + \left(\frac{2\lambda z_o}{\pi}\right)^{1/2}\left[1-\exp\left(-\frac{x_o^2}{2\lambda z_o}\right)\right]\right\} \tag{6}$$

The possible solutions Φ corresponding to the imposed layer deformation caused by dislocation distributions (or disclination quadrupole) will now be discussed. The minimization of expression (1) with respect to the displacement u and the angle Φ gives two equilibrium equations which, using the equation (2) together with the supposed condition $\partial u_d/\partial y = 0$, lead to the following two equations for the angle Φ:

$$\frac{\partial}{\partial y}\left[C_1\frac{\partial^2\Phi}{\partial x^2} + C_2\frac{\partial^2\Phi}{\partial y^2}\right] = 0 \tag{7a}$$

and

$$B_1\left[\frac{\partial^2\Phi}{\partial x^2} + \frac{\partial^2\Phi}{\partial y^2}\right] + B_3\frac{\partial^2\Phi}{\partial z^2} = 0 \tag{7b}$$

The condition (7 *a*) gives the relation $\partial\Phi/\partial y = 0$ [19]. The equation (7 *b*) should be discussed together with the anchoring energy W_s per unit surface area, which can be represented in the form:

$$W_s = W_M \sin^2\Phi \pm W_o\cos\Phi \tag{8}$$

where W_M and W_o are positive. The polar term $\pm W_o\cos\Phi$ should be taken with the sign (+) at the upper surface and with (−) at the lower surface.

As discussed in [19], the layer deformation connected with the horizontal chevron together with the anchoring energy W_s lead to the homogeneous director orientation characterized by the angle $\Phi = 0$. In this case the director $\mathbf{t} = (1, 0, 0)$ is parallel to the x-axis and perpendicular to dislocation or disclination lines. In a non-chiral SmC such a director orientation seems to be energetically non-favourable [20]. But in a chiral SmC* with the molecular spontaneous polarization $\mathbf{P}_s$, perpendicular to the director $\mathbf{t}$, dislocations are not charged when $\mathbf{P}_s$ is parallel to defects [21]. Therefore in a SmC* the director orientation with $\Phi = 0$ will be preferred along the whole sample thickness. However, in the vicinity of sample surfaces the observed situation could be different from this model because we neglected the influence of the surface on the dislocation which terminates at it.

The conclusion from the above discussion, i.e. the director orientation with $\Phi = 0$, is valid only when our assumptions are satisfied, i.e. near dislocation walls and near coherent walls where the layer deformation is concentrated. For example, at distances from coherent walls, typically greater then $2(\lambda z_o)^{\frac{1}{2}}$, the deformation of smectic layers is less important. Therefore it can be supposed that locally there is no layer displacement, i.e. $u = 0$. Then equation (7 *a*) is irrelevant and equation (7 *b*), which is now valid for any Φ, permits, for example, the solution $\Phi = (\pi/2)(1+2y/D)$, describing the **t**-vector twist between the upper sample surface at $y = D/2$ and the lower surface at $y = -D/2$. Such twist can exist in thicker samples with $D > D_c \approx \pi^2 B_2/4W$ [22] where the twist deformation energy is smaller than the polar anchoring energy W_o.

4.2. *Proper energies of coherent and incoherent walls*

As mentioned in the previous section, the energy E_Q does not contain the proper wall energies. Let the coherent wall have the proper energy (per unit of the wall surface) γ_c and the proper incoherent wall energy γ_i. Then the total energy of twist domain E_d in the sample of thickness D is in our approximation:

$$E_d = D\left(E_Q + 4z_o\gamma_c + 4x_o\gamma_i\right). \tag{9}$$

4.2.1. Energy of the coherent wall. The energy γ_c of the so called coherent wall is mainly the layer deformation

Downloaded At: 15:54 25 January 2011

energy which is concentrated principally at the wall thickness ζ determined by Kléman and Lavrentovich [11] as $\zeta=2\lambda/\tan\theta$. With $\lambda\approx0.003\,\mu m$ and $\theta=36^\circ$ the wall thickness is typically $\zeta\approx0.01\,\mu m$, which is of the same order as the interface thickness of the vertical chevron [23].

In thicker samples twin-like textures usually form stripes separated by elongated coherent walls. Coherent walls are transformed to focal conic domains as discussed in [24]. The critical sample thickness D_c for which the transformation of a coherent wall to a focal domain is favourable can be estimated as in [11]. Let the part of the coherent wall with the surface $(4ab)$ be transformed into a focal domain whose ellipse has major and minor semiaxes denoted as a and b, respectively. The hyperbola of the focal domain is generally in the direction of the smectic layer normals. Therefore the relationship between parameters a and b and the tilt angle θ is in the form [24]:

$$(b/a)^2=\sin^2\theta.$$

The focal conic energy [11, 25] per area $(4ab)$ is:

$$\frac{1}{4ab}\left[4\pi K\left(1-e^2\right)K\left(e^2\right)a\ln\frac{a}{r_c}+a\alpha(a,b)E_{core}\right] \quad (10)$$

where $e^2=1-(b/a)^2$, $K(e^2)$ is the complete elliptic function of the first kind, and r_c is the core radius. The parameter E_{core} is the core energy per unit length of focal conic singularities and the geometric factor $\alpha(a, b)$ is related to the lengths of an ellipse and part of a hyperbola situated within a volume a^3. This approximates to

$$\alpha(a,b)=\pi\left[\frac{3}{2}\left(1+\frac{a}{b}\right)-\left(\frac{b}{a}\right)^{\frac{1}{2}}\right]+\left[1+\left(\frac{a}{b}\right)^2\right]^{\frac{1}{2}}. \quad (11)$$

The second term in equation (11) is the length of the essential part of the hyperbola approximated by the lengths of its asymptotes $y=\pm bx/a$, between $y=0$ and $y=\pm a/2$.

The energy of equation (10) can be compared with the energy of the coherent wall γ_c determined in [11] as:

$$\gamma_c=(2K/\lambda)(\tan\theta-\theta)\cos\theta. \quad (12)$$

If we further suppose that the ellipse of the focal-domain fits to the sample thickness D, i.e. $D\approx2b$, a comparison of energies (10) and (12) gives an approximate estimate of the critical sample thickness D_c in the form:

$$D_c\approx2b=\frac{\lambda}{(\tan\theta-\theta)\cos\theta}\left[\pi\sin^2\theta\,K\left(e^2\right)\ln\frac{a}{r_c}+\frac{E_{core}}{K}\alpha(a,b)\right]. \quad (13)$$

In this approximation the elastic constant K is the SmA limit of the previously introduced elastic constants A_{11}, A_{12} and A_{21}; typically $K\approx10^{-11}$ N.

The core energy of the singularity can be estimated as $E_{core}=2\pi r_c\gamma_o$ [26] which is based on the notion of a hollow core of the radius r_c with the inner surface having surface energy γ_o. For $\gamma_o\approx2.5\times10^{-2}\,J\,m^{-2}$, which is a typical value of the smectic A surface energy [26], and with $r_c\approx0.001\,\mu m$ we obtain the ratio $E_{core}/K\approx16$. The estimation of D_c from equation (13), with $\ln(a/r_c)\approx3\ln10$, gives $D_c\approx2.3\,\mu m$. For thicknesses $D>D_c$ the focal domain has a lower energy than 2D-incoherent wall so the transformation is possible. This does not mean that this transformation is always realized for samples of critical thickness because equation (13) is a simplified estimate where, for example, the influence of sample surfaces is not taken into account.

4.2.2. Energy of the incoherent wall. The energy γ_i of the incoherent wall can be either the core energy of the edge dislocation distribution, which models the incoherent wall in thin samples, *or* an array of small focal conics. Experimental observations in SmC* samples, figures 1 (*a*), 1 (*b*), 2, 3, 4 (*a–c*), show that the length of a coherent wall is greater than the length of an incoherent wall, $z_o>x_o$. Therefore it can be expected that $\gamma_i>\gamma_c$. The energy of an incoherent wall γ_i is the core energy E_{core} of the dislocation distribution, i.e. $\gamma_i=E_{core}/d$. Using $d\approx(b_o/2)\cot\theta$ the supposed inequality $\gamma_i>\gamma_c$, with γ_c given by equation (12), leads to the inequality $\lambda E_{core}/b_oK>0.2$ for all angles θ in the interval $0\leqslant\theta<\pi$. As explained by Kléman [14], elementary edge dislocations of the same sign group themselves to make a dislocation with a greater Burgers vector composed of n smectic layers, i.e. $b_o\approx na_o$. Their distance then becomes $l\approx(na_o/2)\cot\theta$. The optical observations of a thin sample show the thick contrast of incoherent walls. This contrast could be associated with edge dislocations having a Burgers vector greater then the Burgers vector a_o of an elementary edge dislocation. The ratio E_{core}/K is then:

$$\lambda\,E_{core}/a_o\,n\,K>0.2. \quad (14)$$

Let the core energy of a dislocation be identified with the core energy of a focal defect. In the SmC* case the inequality (14) can be satisfied for a small number of layers n. In a non-chiral SmC the coherent and incoherent walls have a comparable length. Therefore we can suppose that $\gamma_i\approx\gamma_c$, which gives an estimation of n as $n\approx80$–100. The corresponding Burgers vector is about 0.1 μm; this could be reason why incoherent walls in a SmC are thicker.

Downloaded At: 15:54 25 January 2011

5. Conclusions

The first part of this paper gives an overview of texture observations which appear in SmC* and SmC materials exhibiting N*–SmC* and N–SmC transitions, respectively. While in very thin samples twin-like domains have well defined coherent walls along the anchoring direction, with increasing thickness the twin domains change their shape. Domains are transformed into a system of walls and stripes with no incoherent walls. At greater thickness, coherent walls start to transform into a system of focal conics in order to decrease the surface energy [11].

At further increased thickness, some observations indicate the existence of vertical chevrons of opposite inclination (with respect to the cover glasses). Opposing chevrons are connected in the sample bulk by a system of thick defects. These chevrons can also be transformed into bend walls.

In this paper we construct a model for twin-like domains in very thin samples, because the coherent walls are well defined without the additional structure observed in thicker samples. The elastic model of a twin-like domain is analogous to the model of a twin of rectangular cross-section in solids [18]. It consists of two walls of a continuous distribution of elementary edge dislocations with constant density. The dislocation walls lead to a smectic layer inclination inside a twist-like domain by an angle 2θ. The layer inclination is described by the combination of solutions given by equation (3). The sharp change of layer inclination is also seen in coherent walls which can be called either horizontal chevron interfaces [5, 8] or curvature walls [11].

The original formulation of the model was made for the smectic A phase [13]. The model is useful for the description of elastic layer deformation inside and outside the twin domain both in SmC* and SmC phases, but far from the walls. The deformation inside a coherent wall, and associated proper energy of this wall, were determined in [11]. This evaluation of the proper energy of a coherent wall can be applied to the case of thin samples. In thicker samples the transformation of a coherent wall into a system of focal conics should be considered. In that case the energy γ_c can be estimated with the use of equation (10). It should be noted, however, that the core energy of a focal defect was estimated using the notion of the hollow core as applied to the case of edge dislocation [25]. This estimation gives a higher core energy, of the order of $\sim$10 K. The usual estimation supposing melted smectic in the core is about $\sim$1 K per unit length of core [27]. The estimation of the proper energy of incoherent walls is based on the edge dislocation self-energy as given in the § 4.2.

Twin-like domains are created during the first order transition due to the possibility of $\pm\theta$ inclination of the layer normal from the anchoring direction. The domains are stabilized by barriers which prevent the free motion of coherent and incoherent walls. The motion of coherent walls is discussed by Dierking [5]. The application of an asymmetric a.c. electric field leads to material flow along wall [28] and therefore to wall motion in the direction of the wall normal. This mechanism of wall motion can lead to the elimination of twin-like domain. The motion of an incoherent wall is the dislocation motion perpendicular to smectic layers. Similarly, as in solids, this type of motion is prevented by the so-called Peierls–Nabarro barrier [9, 26] so that external fields are also needed to move an incoherent wall. On the other hand, the application of a d.c. electric field leads to spontaneous polarization switching in a SmC*, i.e. to molecular reorientation only, without apparent wall motion.

Acknowledgement

One of the authors (L.L.) would like to acknowledge the hospitality of the Université Montpellier II.

References

[1] J.S. Patel, S.-D. Lee, J.W. Goodby. *Phys. Rev., A*, **40**, 2854 (1989).
[2] J.S. Patel, J.W. Goodby. *J. appl. Phys.*, **59**, 2355 (1986).
[3] T. Hatano, K. Yamamoto, H. Takezoe, A. Fukuda. *Jpn. J. appl. Phys.*, **25**, 1762 (1986).
[4] I. Dierking, L. Komitov, S.T. Lagerwall. *Ferroelectrics*, **211**, 259 (1998).
[5] I. Dierking. *Textures of liquid crystals*. Wiley-VCH, Weinheim (2003).
[6] I. Dierking, F. Gießelmann, J. Schadt, P. Zugenmaier. *Liq. Cryst.*, **19**, 179 (1995).
[7] A. Jákli, A. Saupe. *Phys. Rev. A*, **45**, 5674 (1992).
[8] N.A. Clark, T.P. Rieker, J.E. Maclennan. *Ferroelectrics*, **85**, 467 (1988).
[9] J.P. Hirth, J. Lothe. *Theory of Dislocations*. McGraw-Hill, New York (1968).
[10] K. Myojin, H. Moritake, M. Ozaki, K. Yoshino, T. Tani, K. Fujisawa. *Jpn. J. appl. Phys.*, **33**, 5491 (1994).
[11] M. Kléman, O. Lavrentovich. *Soft Matter Physics – An Introduction*. Springer, New York (2003).
[12] P.G. de Gennes, J. Prost. *The Physics of Liquid Crystals* 2nd Edn, Clarendon Press, Oxford (1993).
[13] L. Lejček. *Czech. J. Phys.*, **B40**, 1250 (1990).
[14] M. Kléman. *Points, Lines, and Walls in Liquid Crystals, Magnetic Systems and Various Ordered Media*. J. Wiley, New York (1983).
[15] I. Dozov. *Phys. Rev. Lett.*, **74**, 4245 (1995).
[16] P.G. de Gennes. *C.R. Acad. Sci. Paris*, **B275**, 939 (1972).
[17] M. Allain, M. Kléman. *J. Physique*, **48**, 1799 (1978).
[18] F. Kroupa, L. Lejček. *Czech. J. Phys.*, **B20**, 1063 (1970).
[19] L. Lejček, S. Pirkl. *Liq. Cryst.*, **8**, 871 (1990).
[20] L. Bourdon. Thesis, Université Pierre et Marie Curie, Paris, France (1980).

Downloaded At: 15:54 25 January 2011

[21] R. Holyst, A. Poniewierski, P. Fortmeier, H. Stegemayer. *Phys. Rev. Lett.*, **81**, 5848 (1998).
[22] J. Pavel. *J. Physique*, **45**, 137 (1984).
[23] T.P. Rieker, N.A. Clark, G.S. Smith, D.S. Parmer, E.B. Sirota, C.R. Safinya. *Phys. Rev. Lett.*, **59**, 2658 (1987).
[24] C.E. Williams. PhD thesis, Orsay: Université Paris XI, France (1976).
[25] M. Kléman. *J. Physique*, **38**, 1511 (1977).
[26] P. Oswald, P. Pieranski. *Nematic and Cholesteric Liquid Crystals*. CRC Press and Taylor & Francis Group, Boca Raton (2005). *Smectic and Columnar Liquid Crystals*, CRC Press and Taylor & Francis Group, Boca Raton (2006).
[27] J.B. Fournier, G. Durand. *J. Phys. II Fr.*, **1**, 845 (1991).
[28] I. Dierking. *Ferroelectrics*, **234**, 171 (1999).

Downloaded At: 15:54 25 January 2011